49th AIAA Aerospace Sciences Meeting including the New Horizons Forum and Aerospace Exposition
4 - 7 January 2011, Orlando, Florida

AIAA 2011-781

Assessment of Presumed PDF Models for Large Eddy Simulation of Turbulent Premixed Flames

Nasim Shahbazian [*] , Clinton P.T. Groth [†] and Ömer L. Gülder [‡]

University of Toronto Institute for Aerospace Studies

4925 Dufferin Street, Toronto, ON, M3H 5T6, Canada

Large Eddy Simulation (LES) of a freely propagating turbulent premixed flame and Bunsen-type turbulent premixed flame has been carried out using the Presumed Conditional Moment, Flame Prolongation of ILDM (PCM-FPI) approach. Three different presumed probability density functions (PDF) for the reaction progress variable are examined: a beta-PDF, a PDF based on laminar flamelets, and a modified form of the latter. The tabulated data and the predicted LES solutions for the freely propagating flame configuration were compared using the beta-PDF and modified laminar flame-based PDF. It is shown that the laminar flame-based PDF is not applicable in the present study where the flame is in the thin reaction zone regime. The tabulated data based on the solution of one-dimensional laminar flames shows higher reaction rate for the beta-PDF compared to the modified laminar flame-based PDF for high values of segregation factor. This is confirmed by comparison of turbulent burning rate in the predicted LES results where the burning rate for beta-PDF is higher than the modified laminar flame based PDF. For the major species, such as CO and CO_2 for the two PDFs did not show any obvious difference, both in the tabulated data and for the LES solutions. However, for minor species such as H, OH and H_2, the differences are more significant, especially for high segregation factors. Direct numerical simulation (DNS) of a freely propagating turbulent premixed flame is also presented and compared to the predicted LES solutions obtained using the beta-PDF and modified laminar flame-based PDF approaches. For the Bunsen-type burner configuration, results have been obtained using the PCM-FPI approach with the β-PDF and modified laminar flame-based PDF. The results show good agreement with the experimental data and provide a good evaluation of the PCM-FPI method and the influence of presumed PDF on LES results for premixed flames.

I. Introduction

Turbulent premixed flames are widely used in industrial applications. The necessity of pollution control, increasing efficiency and decreasing fuel consumption in combustion engines highlights the importance of premixed flame studies. Due to difficulties of studying the flame structure experimentally, numerical simulations have become a powerful tool for understanding of the flame behaviour. However, the complex interactions between turbulence and chemical species in various scales and short combustion times, prevent numerical methods to fully explain the experimental observations.

Accurate modelling of the reaction rate is the objective of many numerical studies of turbulent flames. The main problem in Large Eddy Simulation (LES) of reacting flows is that the flame thickness is generally much smaller than the LES mesh size, Δ. So the progress variable is a very stiff function of space and the flame front cannot be resolved by the LES grid. Different approaches are used for the reaction rate modelling. One approach is statistical models which used a presumed probability density function (PDF).[1] The effect of chemical mechanism can be included using tabulated data. The Flame Prolongation of ILDM (FPI) method has been developed by Gicquel et al.[2] to include detailed chemistry effects without solving all species mass fraction equations. In this method, datasets of flame quantities are tabulated using the

[*]Ph.D. Candidate, shahbazian@utias.utoronto.ca
[†]Professor, Senior Member AIAA, groth@utias.utoronto.ca
[‡]Professor, Senior Member AIAA, ogulder@utias.utoronto.ca

properties of unstrained, one-dimensional laminar premixed flames. The Presumed Conditional Moment with tabulated chemistry (PCM-FPI) approach is an attractive method for LES. However, the sensitivity of this method to the presumed probability density function of progress variable is rarely discussed. A β-PDF is generally used as the presumed probability density function for the progress variable in both premixed and non-premixed flames.[3–6] This PDF produces the correct bimodal and monomodal shapes at large and small variances respectively.[7] Domingo et al.[8] used FPI with a combination of presumed PDF based on the gradient of progress variable for the regions inside the flame. However, this alternative PDF is only valid for high values of variances and Domingo et al.[8] recommended switching to the β-PDF for the low values of subgrid scale variance. Bray et al.[7] examined three PDFs for the progress variable: a β-PDF, an interior PDF provided by laminar flamelets and PDF based on delta functions for a case with a high subgrid scale variance. They found better agreement between the laminar flamelet PDF and the Direct Numerical Simulation (DNS) data. More recently, Jin et al.[9] used different PDFs in combination with a Conditional Source-term Estimation (CES) model and compared their results with the DNS data. They introduced a modified laminar flame-based PDF which is applicable for all ranges of subgrid scale variances and therefore also applicable to turbulent flames lying within the thin reaction zone regime. They reported better agreements between this PDF and DNS data.

In the present study, a β-PDF, the Bray et al.[7]'s laminar flame-based PDF and the modified laminar flame-based PDF introduced by Jin et al.[9] are all considered for integrating and obtain filtered quantities using the FPI flamelet tabulation. The LES results for premixed flames are compared to both DNS and experimental data for a simple canonical flame propagation problem as well as a laboratory scale Bunsen configuration, respectively.

II. Favre-Filtered Governing Equations

The objective of LES is to explicitly compute the scales of the flow which are larger than the filter size, Δ, and model the remaining smaller scales. Solution quantities, Q, are generally filtered, $\bar{Q}$ or Favre-filtered, $\tilde{Q}$ in the physical space. Using this procedure, the Favre-filtered mass, momentum, total energy, chemical species transport and state equations for a thermally perfect reactive mixture of gases are given by

$$\frac{\partial \bar{\rho}}{\partial t} + \frac{\partial (\bar{\rho}\tilde{u}_j)}{\partial x_j} = 0 \tag{1}$$

$$\frac{\partial (\bar{\rho}\tilde{u}_i)}{\partial t} + \frac{\partial (\bar{\rho}\tilde{u}_i\tilde{u}_j + \delta_{ij}\bar{p})}{\partial x_j} - \frac{\partial \check{\tau}_{ij}}{\partial x_j} = \underbrace{-\frac{\partial \sigma_{ij}}{\partial x_j}}_{\mathbf{I}} + \underbrace{\frac{\partial (\bar{\tau}_{ij} - \check{\tau}_{ij})}{\partial x_j}}_{\mathbf{II}} \tag{2}$$

$$\begin{aligned}\frac{\partial (\bar{\rho}\tilde{E})}{\partial t} + \frac{\partial [(\bar{\rho}\tilde{E} + \bar{p})\tilde{u}_j]}{\partial x_j} - \frac{\partial (\check{\tau}_{ij}\tilde{u}_i)}{\partial x_j} + \frac{\partial \check{q}_j}{\partial x_j} \quad = \quad & \underbrace{-\frac{\partial [\bar{\rho}(\widetilde{u_j h_\mathrm{s}} - \tilde{u}_j \check{h}_\mathrm{s})]}{\partial x_j}}_{\mathbf{III}} \\ & + \underbrace{\frac{\partial (\bar{\tau}_{ij}\tilde{u}_i - \check{\tau}_{ij}\tilde{u}_i)}{\partial x_j}}_{\mathbf{IV}} + \underbrace{\frac{\partial (\overline{u_i \tau_{ij}} - \tilde{u}_i \bar{\tau}_{ij})}{\partial x_j}}_{\mathbf{V}} \\ & \underbrace{- \frac{1}{2}\frac{\partial [\bar{\rho}(\widetilde{u_j u_i u_i} - \bar{\rho}\tilde{u}_j \widetilde{u_i u_i})]}{\partial x_j}}_{\mathbf{VI}} + \underbrace{\frac{\partial (\bar{q}_j - \check{q}_j)}{\partial x_j}}_{\mathbf{VII}} \\ & \underbrace{- \frac{\partial [\sum_{n=1}^{N} \Delta h^0_{\mathrm{f},n} \bar{\rho}(\widetilde{Y_n u_j} - \tilde{Y}_n \tilde{u}_j)]}{\partial x_j}}_{\mathbf{VIII}}\end{aligned} \tag{3}$$

$$\frac{\partial (\bar{\rho}\tilde{Y}_n)}{\partial t} + \frac{\partial (\bar{\rho}\tilde{Y}_n\tilde{u}_j)}{\partial x_j} + \frac{\partial \check{\mathcal{J}}_{j,n}}{\partial x_j} = \underbrace{-\frac{\partial [\bar{\rho}(\widetilde{Y_n u_j} - \tilde{Y}_n\tilde{u}_j)]}{\partial x_j}}_{\mathbf{IX}} - \underbrace{\frac{\partial (\bar{\mathcal{J}}_{j,n} - \check{\mathcal{J}}_{j,n})}{\partial x_j}}_{\mathbf{X}} + \underbrace{\bar{\dot{\omega}}_n}_{\mathbf{XI}} \tag{4}$$

$$\bar{p} = \bar{\rho} R \tilde{T} + \underbrace{\sum_{n=1}^{N} R_n \bar{\rho} (\widetilde{Y_n T} - \tilde{Y}_n \tilde{T})}_{\textbf{XII}} \tag{5}$$

where $\bar{\rho}$ is the filtered mixture density, $\tilde{u}_i$ is the Favre-filtered mixture velocity, $\bar{p}$ is the filtered mixture pressure, $\tilde{Y}_n$ is the Favre-filtered mass fraction of species n, N is the total number of species, $\bar{\dot{\omega}}_n$ is the filtered reaction rate of species n, R_n and R are the gas constant of species n and the gas constant of the mixture respectively and $\tilde{E}$ is the Favre-filtered total mixture energy which is given by

$$\tilde{E} = \check{h}_\mathrm{s} - \frac{\bar{p}}{\bar{\rho}} + \sum_{n=1}^{N} \Delta h^0_{\mathrm{f},n} \tilde{Y}_n + \frac{1}{2} \tilde{u}_i \tilde{u}_i + \tilde{k} \,, \tag{6}$$

where $\check{h}_\mathrm{s}$ and $\Delta h^0_{\mathrm{f},n}$ are the sensible enthalpy and heat of formation for species n respectively and $\tilde{k}$ is the subfilter scale turbulent kinetic energy and is defined as

$$\tilde{k} = \frac{1}{2} (\widetilde{u_i u_i} - \tilde{u}_i \tilde{u}_i) \,. \tag{7}$$

The subfilter-scale stress tensor is given by

$$\sigma_{ij} = -\bar{\rho} (\widetilde{u_i u_j} - \tilde{u}_i \tilde{u}_j) \,, \tag{8}$$

and

$$\check{\tau}_{ij} = 2\check{\mu} (\tilde{S}_{ij} - \frac{1}{3} \delta_{ij} \tilde{S}_{ll}) \,, \tag{9}$$

$$\check{q}_j = -\check{\kappa} \frac{\partial \tilde{T}}{\partial x_j} - \bar{\rho} \sum_{n=1}^{N} \check{h}_n \check{D}_n \frac{\partial \tilde{Y}_n}{\partial x_j} \,, \tag{10}$$

$$\check{\mathcal{J}}_{j,n} = \bar{\rho} \check{D}_n \frac{\partial \tilde{Y}_n}{\partial x_j} \,, \tag{11}$$

are the viscous stress tensor, heat flux, and species molecular flux, respectively, which are evaluated in terms of the filtered quantities. The tensor $\tilde{S}_{ij} = \frac{1}{2}(\partial \tilde{u}_i / \partial x_j + \partial \tilde{u}_j / \partial x_i)$ is the strain rate tensor corresponding to the filtered velocities, and $\check{\mu}$, $\check{\kappa}$ and $\check{D}_n$ are the molecular viscosity, thermal conductivity and molecular diffusivity of species n, corresponding to values at $\tilde{T}$.

III. Subgrid Scale Models

In preceding set of filtered equations given above, the unclosed quantities (terms **I** to **XII**) must be modelled. It can be assumed that the filtered viscous stresses $\bar{\tau}_{ij}$, total heat fluxes $\bar{q}_j$ and species fluxes $\bar{\mathcal{J}}_{j,n}$ are approximated by $\check{\tau}_{ij}$, $\check{q}_j$ and $\check{\mathcal{J}}_{j,n}$ respectively. As a result, terms **II**, **IV**, **VII** and **X** may be neglected. Subfilter scale viscous diffusion (term **V**) is much smaller than the other terms in the equation and so it can be neglected.[10] The subfilter temperature-species correlation term (term **XII**) is also generally neglected. Furthermore, the subfilter scale turbulent diffusion (term **VI**) is modelled here as[11]

$$-\frac{\bar{\rho}(\widetilde{u_j u_i} u_i - \bar{\rho} \tilde{u}_j \widetilde{u_i u_i})}{2} = \sigma_{ij} \tilde{u}_i \,. \tag{12}$$

A. Modelling of Subgrid Stresses

In this work, a k-equation model is considered as a subfilter eddy-viscosity model to represent the subfilter stresses. In this model, an additional transport equation for $\tilde{k}$ is solved. The subgrid scale stresses are modelled as

$$\sigma_{ij} = 2\bar{\rho}\nu_\mathrm{t} \left(\check{S}_{ij} - \frac{1}{3} \delta_{ij} \check{S}_{ll} \right) - \bar{\rho} \frac{2}{3} \delta_{ij} \tilde{k} \,, \tag{13}$$

where the subfilter eddy viscosity is defined as

$$\nu_\mathrm{t} = C_\mathrm{v} \sqrt{k} \Delta. \tag{14}$$

The coefficient C_v is approximately between 0.086 and 0.09. The modelled transport equation for the subfilter kinetic energy, $\tilde{k}$, is given by

$$\frac{\partial(\bar{\rho}\tilde{k})}{\partial t} + \frac{\partial(\bar{\rho}\tilde{k}\tilde{u}_i)}{\partial x_i} = P - \epsilon + \frac{\partial}{\partial x_i}\left(\bar{\rho}\frac{\nu_\mathrm{t}}{Pr_\mathrm{t}}\frac{\partial\tilde{k}}{\partial x_i}\right), \tag{15}$$

where Pr_t is the subfilter scale turbulent Prandtl number and is typically between 0.7 to 0.9. The production P, and dissipation ϵ, terms are respectively given by

$$\begin{aligned} P &= \sigma_{ij}\check{S}_{ij}, \\ \epsilon &= C_\epsilon\bar{\rho}k^{3/2}/\Delta, \end{aligned}$$

where C_ϵ is approximately between 0.845 to 1.0.

B. Modelling of Subgrid Sensible Enthalpy and Scalar Fluxes

Subgrid scalar fluxes and subgrid sensible enthalpy fluxes are generally closed using classical gradient assumptions, such that

$$\bar{\rho}(\widetilde{Y_n u_j} - \tilde{Y}_n\tilde{u}_j) = -\frac{\mu_\mathrm{t}}{Sc_\mathrm{t}}\frac{\partial\tilde{Y}_n}{\partial x_j}. \tag{16}$$

$$\bar{\rho}(\widetilde{u_j h_\mathrm{s}} - \tilde{u}_j\check{h}_\mathrm{s}) = -\frac{\check{C}_\mathrm{p}\mu_\mathrm{t}}{Pr_\mathrm{t}}\frac{\partial\tilde{T}}{\partial x_j}, \tag{17}$$

where $\check{C}_\mathrm{p}$ is the mixture specific heat at constant pressure and Sc_t is the subfilter scale turbulent Schmidt number which is used to relate the transport of the scalar to the momentum transport. The value of Sc_t is usually taken in the range of 0.7 to 0.9.

IV. Presumed Conditional Moment with Tabulated Chemistry

To include detailed chemistry effects without solving for all species transport equations, the FPI tabulation method proposed by Gicquel et al.[2] is used. In this approach, all flame quantities are related to a single progress variable, Y_c which should be chosen carefully so that there exists a one-to-one correspondence between Y_c and each flame solution quantity.[4] For methane-air combustion, which is of primary interest here, $Y_\mathrm{c} = Y_\mathrm{CO} + Y_{\mathrm{CO}_2}$ is a suitable choice.[12,13] Numerical solutions for a set of one-dimensional, unstretched, freely propagating, laminar, premixed flames are computed with the GRI-Mech 3.0 mechanism[14] and the flame quantities are stored in a look-up table in terms of reaction progress variable Y_c, and a mixture fraction characterizing the equivalence ratio, ϕ_0. Any flame property, φ^P, (species mass fractions, reaction rates, etc.) of unstrained premixed flames at an equivalence ratio, (ϕ_0), may be tabulated either in (x, ϕ_0) or in (Y_c, ϕ_0). The FPI table is then written as[15]

$$\varphi_j^\mathrm{FPI}(\phi_0, Y_\mathrm{c}) = \varphi_j^\mathrm{P}(\phi_0, x). \tag{18}$$

For turbulent premixed flames, the effect of turbulence on the combustion can then be incorporated via a presumed probability density function for the progress variable, c. A filtered property for species i, φ_i can be calculated using the probability density function as follows

$$\tilde{\varphi}_i = \int_{c^*} \varphi_i(c^*)\tilde{P}(c^*)\mathrm{d}c^*. \tag{19}$$

Several forms of presumed probability density functions (PDF) have been used with FPI method which all depend on mean, $\bar{c}$ and variance, $\overline{c''^2}$ of reaction progress variable. These PDFs are discussed in the next section. Values of $\bar{c}$ and $\overline{c''^2}$ are calculated from the progress of reaction, $\tilde{Y}_\mathrm{c}$ and its subfilter scale variance, Y_cv where $Y_\mathrm{cv} = \widetilde{Y_\mathrm{c}Y_\mathrm{c}} - \tilde{Y}_\mathrm{c}\tilde{Y}_\mathrm{c}$. The progress variable takes the form

$$\bar{c}(\phi_0) = \frac{\tilde{Y}_\mathrm{c}}{\tilde{Y}_\mathrm{c}^\mathrm{eq}(\phi_0)}. \tag{20}$$

The expression for $c_{\rm v}$ is given by

$$c_{\rm v} = \frac{Y_{\rm cv}}{\widetilde{Y_{\rm c}^{\rm eq2}}} + \tilde{Y}_{\rm c}^2 \left(\frac{1}{\widetilde{Y_{\rm c}^{\rm eq2}}} - \frac{1}{\tilde{Y}_{\rm c}^{\rm eq2}} \right) . \tag{21}$$

Balance equations for the means and variances must be solved along with the filtered Navier-Stokes equations. The balance equations for $\tilde{Y}_{\rm c}$ and $Y_{\rm cv}$ take the form

$$\frac{\partial(\bar{\rho}\tilde{Y}_{\rm c})}{\partial t} + \frac{\partial(\bar{\rho}\tilde{u}_i\tilde{Y}_{\rm c})}{\partial x_i} = \frac{\partial}{\partial x_i}\left(\bar{\rho}(D + D_{\rm t}) \frac{\partial \tilde{Y}_{\rm c}}{\partial x_i} \right) + \bar{\rho}\tilde{\dot{\omega}}_{Y_{\rm c}} , \tag{22}$$

$$\begin{aligned} \frac{\partial(\bar{\rho}Y_{\rm cv})}{\partial t} + \frac{\partial(\bar{\rho}\tilde{u}_i Y_{\rm cv})}{\partial x_i} &= \frac{\partial}{\partial x_i}\left(\bar{\rho}(D + D_{\rm t}) \frac{\partial Y_{\rm cv}}{\partial x_i} \right) + 2\bar{\rho}(D + D_{\rm t}) \frac{\partial \tilde{Y}_{\rm c}}{\partial x_i} \frac{\partial \tilde{Y}_{\rm c}}{\partial x_i} \\ &\quad - 2\overline{\rho D \frac{\partial Y_{\rm c}}{\partial x_i} \frac{\partial Y_{\rm c}}{\partial x_i}} + 2\bar{\rho}(\widetilde{Y_{\rm c}\dot{\omega}_{Y_{\rm c}}} - \tilde{Y}_{\rm c}\tilde{\dot{\omega}}_{Y_{\rm c}}) , \end{aligned} \tag{23}$$

where D and $D_{\rm t}$ are laminar and turbulent diffusion coefficients respectively and $\tilde{\dot{\omega}}_{Y_{\rm c}}$ is a source term due to chemistry. The linear relaxation closure is used to close the scalar dissipation terms, $\bar{\chi}_{Y_{\rm c}} = 2\overline{\rho D \frac{\partial Y_{\rm c}}{\partial x_i} \frac{\partial Y_{\rm c}}{\partial x_i}}$ as follows[16]

$$\overline{\rho D \frac{\partial Y_{\rm c}}{\partial x_i} \frac{\partial Y_{\rm c}}{\partial x_i}} = \bar{\rho} D \frac{\partial \tilde{Y}_{\rm c}}{\partial x_i} \frac{\partial \tilde{Y}_{\rm c}}{\partial x_i} + C_{\rm d}^{Y_{\rm cv}} \frac{D_{\rm t}}{\Delta^2} \bar{\rho} Y_{\rm cv} . \tag{24}$$

The normalized variance of c is called segregation factor, S and takes the values between zero and unity. It has the form

$$S_{\rm c} = \frac{c_{\rm v}}{\bar{c}(1 - \bar{c})} ,$$

For a turbulent case, the look-up table of filtered quantities is pre-generated based on $\tilde{\varphi}_j^{\rm FPI}(\phi_0, \bar{c}, S_c)$.

A. Generation of Look-up Tables for Methane-Air Chemistry

Look-up tables of the filtered quantities, $\tilde{\varphi}_j^{\rm FPI}(\phi_0, \bar{c}, S_c)$, is pre-generated using the steady state solution of one-dimensional, unstretched, laminar premixed flames obtained using the Cantera package[17] for a methane-air flame with the GRI-Mech 3.0 mechanism.[14] To control table size, a reduced number of 10 species were selected based on their contribution to mixture mass and energy.[4] The look-up table contains 252 values of $\bar{c}$ and 25 values of S_c. In the present study, the species mass fractions are stored and directly read from the table.

V. Presumed Probability Density Functions for Reaction Progress Variable

Different forms of the presumed probability density functions have been used in combination with FPI for turbulent premixed flames. For very high variances close to $\bar{c}(1-\bar{c})$ which correspond to high Damköhler numbers (defined as the ratio of turbulent time scale to chemical time scale), the flame is behaving as a thin near discontinuous interface between reactants and products. In this case the PDF becomes two delta functions.[8,18] For variances very close to zero, a single delta function located at $\bar{c}$ can represent the PDF. A more general form of the PDF is required for the full range of premixed flames.

The three different forms of the PDFs evaluated in this study are summarized below.

A. β-PDF

The first form of PDF used in this work is the standard β-PDF which is used widely in both premixed and non-premixed flames.[3–6] At small and large values of variances, the β-PDF provides correct monomodal and bimodal PDF shapes respectively.[7] A β-PDF for c can be defined as

$$\bar{P}(c^*) = \frac{c^{*a-1}(1-c^*)^{b-1}}{\int_0^1 c^{+a-1}(1-c^+)^{b-1}{\rm d}c^+} , \tag{25}$$

where

$$a = \bar{c}\left(\frac{\bar{c}(1-\bar{c})}{\overline{c''^2}} - 1\right) \geq 0, \qquad b = a\left(\frac{1}{\bar{c}} - 1\right) \geq 0\,. \tag{26}$$

B. Laminar flame-based PDF

The second form for the presumed PDF considered here was first introduced by Bray et al.[7] and is called a laminar flame-based (LFB) PDF. For this PDF, it is assumed that isosurfaces of the progress variable, c, through the flame front are parallel. So the PDF is only applicable for thin flamelet regime where the Kolmogorov time scale is larger than the characteristic time of a laminar flame. In this case, the interior portion of the PDF is assumed to be inversely proportional to $|\nabla c|$. The PDF is then taken to have the form

$$\bar{P}(c^*) = A\delta(c^*) + Bf(c^*) + C\delta(1-c^*), \tag{27}$$

where $f(c^*)$ is calculated based on the solution of unstrained laminar flame.

$$f(c^*) = \frac{1}{|\nabla c|}. \tag{28}$$

The constants A, B and C are calculated based on the first three moment equations of c

$$1 = \int_0^1 \bar{P}(c^*)\mathrm{d}c^* = A + B\int_\epsilon^{1-\epsilon} f(c^*)\mathrm{d}c^* + C, \tag{29}$$

$$\bar{c} = \int_0^1 c^*\bar{P}(c^*)\mathrm{d}c^* = B\int_\epsilon^{1-\epsilon} c^* f(c^*)\mathrm{d}c^* + C, \tag{30}$$

$$\overline{c^2} = \int_0^1 c^{*2}\bar{P}(c^*)\mathrm{d}c^* = B\int_\epsilon^{1-\epsilon} c^{*2} f(c^*)\mathrm{d}c^* + C, \tag{31}$$

and ϵ is a small number defines the inner zone of premixed flamelet. The coefficients are determined as

$$B = \frac{\bar{c} - \overline{c^2}}{I_1 - I_2}\,, \qquad C = \frac{\overline{c^2}I_1 - \bar{c}I_2}{I_1 - I_2}\,, \qquad A = 1 - BI_0 - C. \tag{32}$$

where I_0, I_1 and I_2 are

$$I_0 = \int_0^1 \frac{1}{|\nabla c^*|}\mathrm{d}c^*\,, \qquad I_1 = \int_0^1 \frac{c^*}{|\nabla c^*|}\mathrm{d}c^*\,, \qquad I_2 = \int_0^1 \frac{c^{*2}}{|\nabla c^*|}\mathrm{d}c^*. \tag{33}$$

These relations fail for negative values of A, B and C. The positivity of these coefficients implies that this subfilter scale presumed PDF is only valid for high values of segregation factor (large variances) or very thin flamelets.[8] Domingo et al.[8] suggested switching to a β-PDF for the points with low variance. For typical flames in the thin reaction zone regime, this leads to using a β-PDF for the entire flame brush rather than the proposed laminar flame-based PDF.

C. Modified laminar flame-based PDF

To overcome this limitation, a modified laminar flame-based (modified LFB) PDF has been proposed by Jin et al.[9] The idea is to use that part of the laminar flame which has the same mean and variance as the turbulence flame and for the rest of the points force $f(c^*)$ to zero. If the progress variable for truncated region in the laminar flame is shown by c_1 and c_2 with positions x_1 and x_2 respectively, and if $c_{\min} = \triangle c/2$ with $x = x_{\min}$ and $c_{\max} = 1 - \triangle c/2$ with $x = x_{\max}$ four possible cases can be written as[9]

1. If $x_{\min} < x_1 < x_2 < x_{\max}$:

$$\bar{P}(c^*) = \begin{cases} 0 & \text{if } c^* < c_1 \text{ or } c^* > c_2 \\ B_1 f(c^*) & \text{if } c_1 \leq c^* \leq c_2 \end{cases}$$

2. If $x_1 < x_{\min} < x_2 < x_{\max}$:

$$\bar{P}(c^*) = \begin{cases} A_2\delta(c^*) + B_2 f(c^*) & \text{if } c^* \le c_2 \\ 0 & \text{if } c^* > c_2 \end{cases}$$

3. If $x_{\min} < x_1 < x_{\max} < x_2$:

$$\bar{P}(c^*) = \begin{cases} 0 & \text{if } c^* < c_1 \\ B_3 f(c^*) + C_3\delta(1-c^*) & \text{if } c^* \ge c_1 \end{cases}$$

4. If $x_1 < x_{\min} < x_{\max} < x_2$:

$$\bar{P}(c^*) = A_4\delta(c^*) + B_4 f(c^*) + C_4\delta(1-c^*), \tag{34}$$

In each case, the values of three of the five parameters of A, B, C, c_1 and c_2 should be determined in terms of the first three moments. All possible distributions of $\bar{P}(c^*)$ are calculated by changing the values of two of these three variables and calculating the third variable so that $\int_0^1 \bar{P}(c^*)\mathrm{d}c^* = 1$. Then for each possible distribution, $\bar{c}$ and $\overline{c'^2}$ are determined. Finally, the value of each property in the FPI table is calculated using these PDFs and tabulated as a function of $\bar{c}$ and $\overline{c'^2}$.[19]

VI. Numerical Solution Scheme

A finite-volume scheme has been developed and used to solve the above Favre-filtered transport equations. The solution method includes parallel high-order central essentially non-oscillatory (CENO) finite volume scheme[20,21] with block-based adaptive mesh refinement (AMR)[22,23] on body-fitted multiblock mesh.[24] However for this study, only the second-order accurate scheme without AMR is used. The code is written for a thermally perfect reactive mixture to account for the viscous stresses and heat flux, as well as varying mixture composition. At each cell face, the inviscid flux is calculated using limited linear reconstruction[25] and Riemann solver or flux-vector-splitting based flux functions.[26,27] The viscous flux is evaluated by a centrally-weighted diamond-path reconstruction method.[28] The dataset of Gordon and McBride[29,30] is used to determine thermodynamic and molecular transport properties of each mixture component. To calculate the molecular viscosity and thermal conductivity of the mixture, the mixture rules of Wilke[31] and Mason and Saxena[32] are used, respectively.

VII. Results and Discussions

A. Comparison of Tabulated Quantities

Figure 1 shows the ranges of the applicability for the laminar flame-based and modified laminar flame-based PDFs respectively. It is clear from Figure 1(a) that the laminar flame-based PDF can only be generated for a limited range of mean and variances. This figure shows that the PDF is only applicable for high Damköhler number flames as also stated by Bray et al.[7] Use of this model for flames in the thin reaction zone regime is certainly not possible. For the modified laminar flame-based, Figure 1(b) shows that this model covers all ranges of mean and variances and therefore can be used for the entire range of premixed flames where the internal flame structure remains largely intact, including the thin reaction zone regime. These results are also consistent with Salehi et al.[19]

The tabulated data for the modified laminar flame-based case is compared with β-PDF in Figures 2, 3 and 4. Figure 2 shows that the values of ω_{Y_c} are similar for both PDFs. For higher segregation factors (equivalent to non-dimensionalized variance), the difference between the two PDFs are more distinct (Figures 2 and 4). Figure 3(a) indicates that for the major species, the choice of β or the modified laminar flame-based PDF does not significantly affect the tabulated values, but the differences become more apparent for minor species such as H (Figure 3(c)) and OH (Figure 4). These results of the comparisons of tabulated values obtained using the different presumed PDFs also agree with the observation of Domingo et al.,[8] who indicated that the prediction of OH is sensitive to the shape of the PDF.

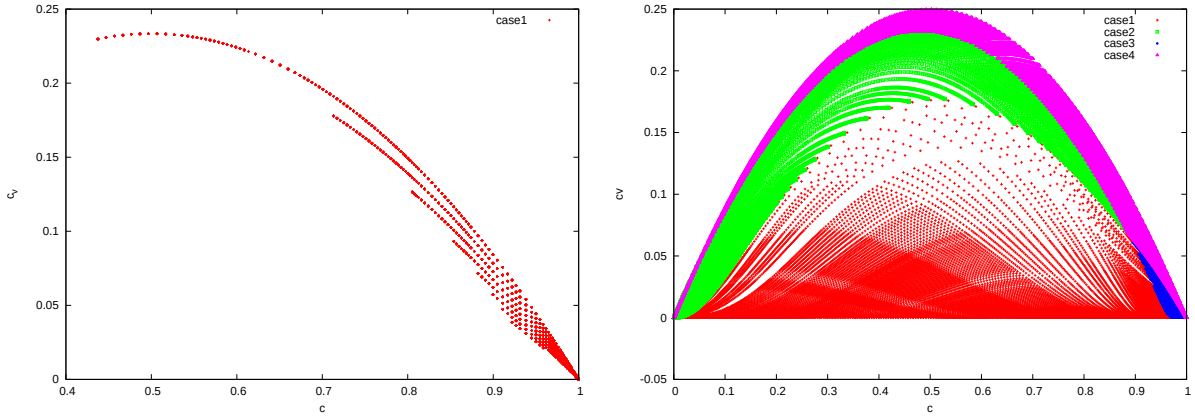

(a) Laminar flame-based PDF (b) Modified laminar flame-based PDF

Figure 1. Range of the applicability of laminar flame-based PDF and each of four possible cases for the modified laminar flame-based PDF for a stoichiometric mixture of methane and air.

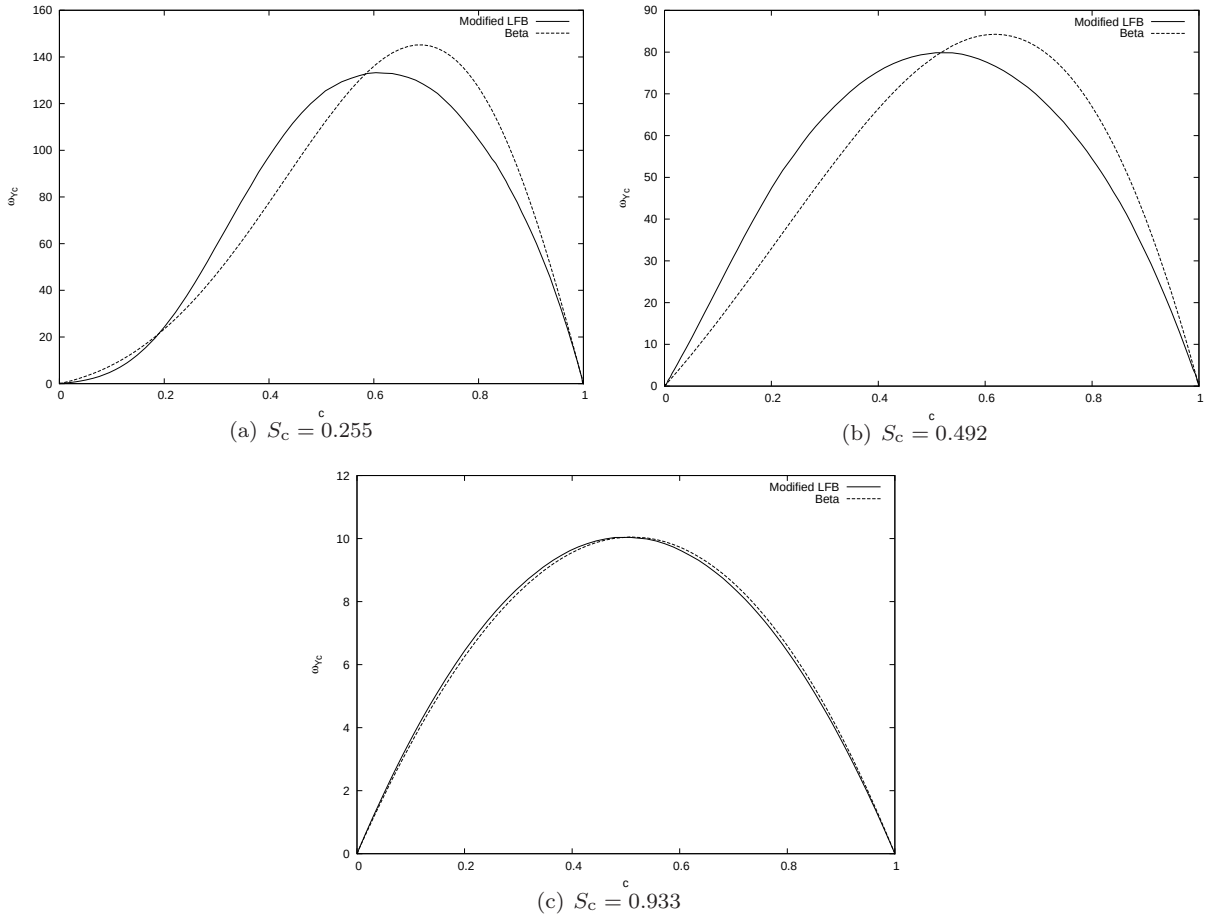

(a) $S_c = 0.255$ (b) $S_c = 0.492$

(c) $S_c = 0.933$

Figure 2. Comparison of tabulated ω_{Y_c} for β-PDF and modified laminar flame-based PDF for a mixture of methane and air at $\phi = 0.7$ in three different segregation factors.

B. Freely Propagating Flame

In order to compare further the effect of the two different PDFs, LES solutions of a freely propagating premixed methane-air flame are studied in a decaying isotropic and homogeneous turbulent field. The flame

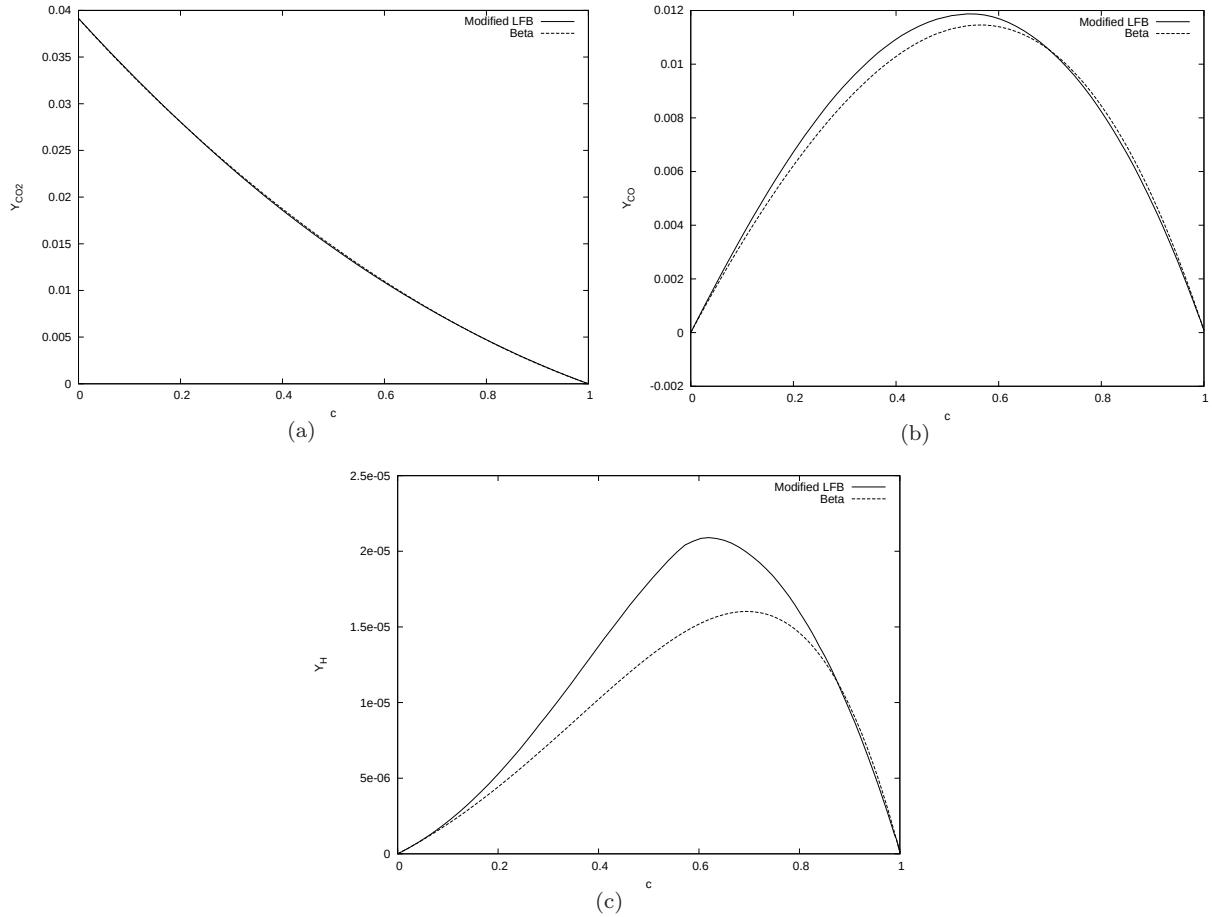

Figure 3. Tabulated mass fraction comparisons for β-PDF and modified laminar flame-based PDF for a mixture of methane and air at $\phi = 0.7$ and $S_c = 0.492$.

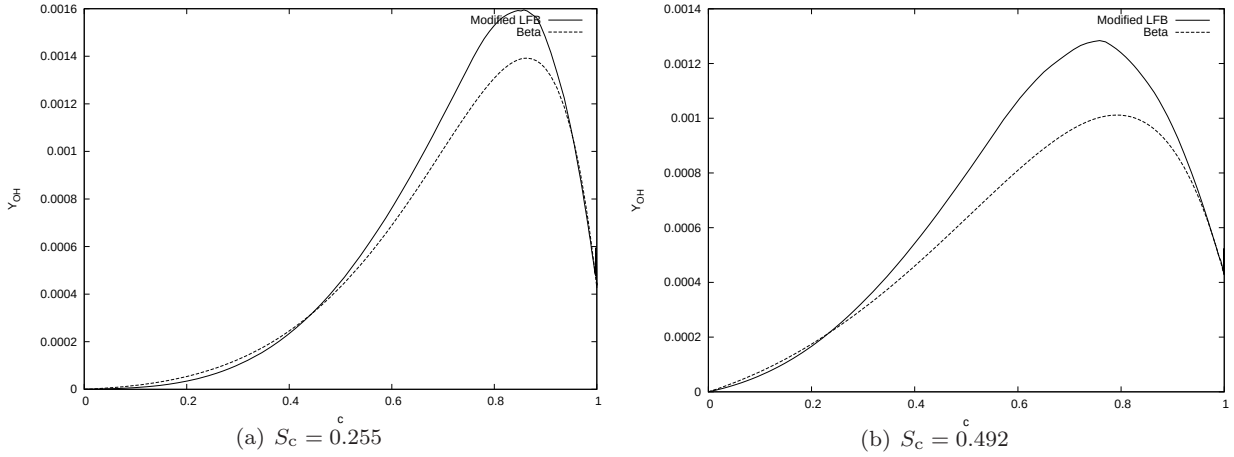

Figure 4. Tabulated Y_{OH} comparisons for β-PDF and modified laminar flame-based PDF for a mixture of methane and air at $\phi = 0.7$ and different segregation factors.

is initialized by a planar laminar premixed flame within a box. A homogeneous isotropic turbulent flow field is superimposed using Rogallo's turbulence initialization procedure[33] and the model spectrum proposed by Pope.[34] Boundary conditions at the six faces of the cube are subsonic inflow and outflow in two directions and periodic for the four other faces. The particular conditions from the premixed flame of interest are summarized in Table 1. The turbulence intensity was such that the flame lies in the thin reaction zone regime of turbulent premixed combustion diagram.[35] The LES results described above is also compared to DNS of the freely propagating flame. For the DNS calculations, a grid of 256^3 is used with the same initial and boundary conditions as the LES case. The analogy used by Aspden et al.[36] is used here in order to examine the ability of the scheme to provide a well-resolved flow simulations. They used dimensional analysis with the theory of Kolmogorov (1941) to define a method known as Implicit Large Eddy Simulation (ILES). From this analysis, an expression for the effective viscosity and therefore effective Kolmogorov length scale, η_e, is defined. They have shown that if the condition, $\eta_e < 1.5\eta$ satisfies, the resolution is sufficient. This ILES condition is satisfied for the present DNS simulation.

ϕ	Λ	λ	η	u'	s_L	δ_L	u'/s_L	$\Lambda/\delta_\mathrm{L}$
	mm	mm	mm	m/s	m/s	mm		
0.7	1.790	0.460	0.02935	2.92	0.201	0.67	14.38	2.67

Table 1. Summary of turbulence scales and flow conditions.

Three-dimensional views of the predicted instantaneous flame surface identified by isosurface of reaction progress variable at $c = 0.5$ and $t = 1\,\mathrm{ms}$ is shown in Figure 5. The LES simulation is performed using β-PDF. The LES results show a highly wrinkled flame with the bigger scale of wrinkles at the tips of the flame. DNS predicts the same wrinkles but with finer structure indicating the effect of the resolved small scales on the flame wrinkling.

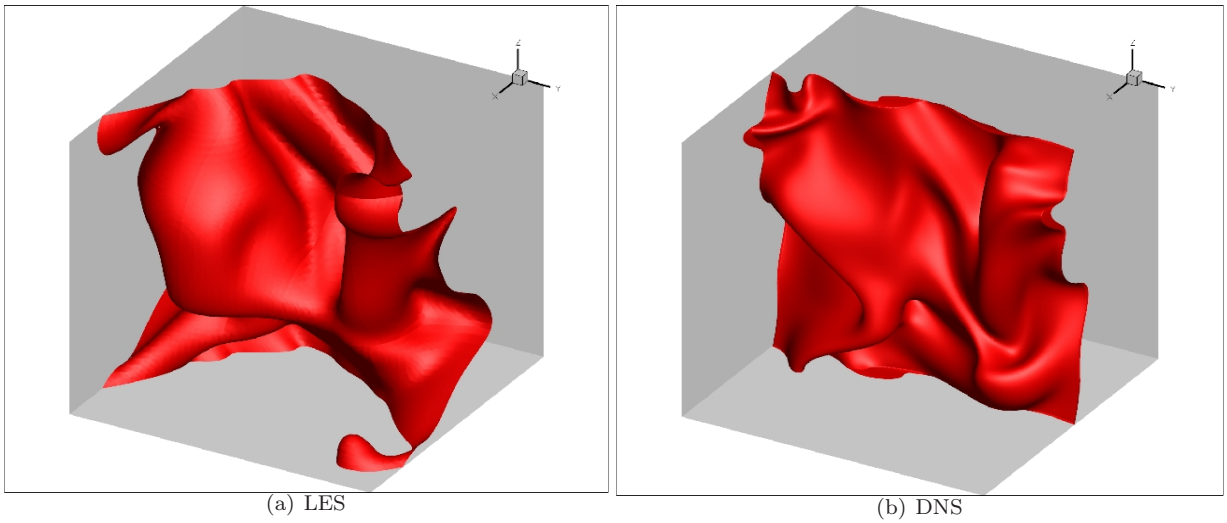

(a) LES (b) DNS

Figure 5. Isosurface of reaction progress variable, $c = 0.5$ for the propagating flame at $t = 1\,\mathrm{ms}$ using LES with β-PDF and DNS.

Figure 6 shows the comparison of burning rate for the cases using the β and modified laminar flame-based PDFs. The expression for the calculation of burning rate in the PCM-FPI model is given by

$$S_\mathrm{T} = \frac{1}{\bar{\rho}_r \tilde{Y}_\mathrm{c}^\mathrm{eq} L_y L_z} \int_V \tilde{\dot{\omega}}_{Y_\mathrm{c}} \mathrm{d}V \tag{35}$$

It is seen that β-PDF produces a slightly higher burning rates than modified laminar flame-based PDF. This agrees with Vicquelin et al.[37] that using a β-PDF over-estimates the propagation speed of the filtered progress variable. DNS calculation of the flame front also agrees with this. As can be seen in the Figure 5, the DNS predicts less wrinkling in general compared to the LES calculations, resulting in a lower burning rate for the flame.

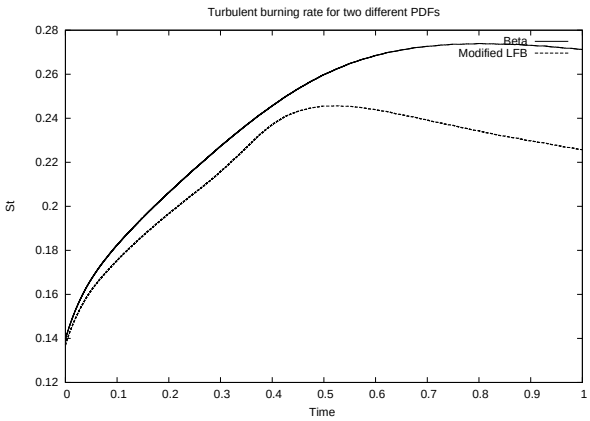

Figure 6. Comparison of turbulent burning rate for β-PDF and modified laminar flame-based PDF.

To compare further the results of two turbulent premixed flames using β-PDF and modified laminar flame-based PDF, the distributions of the reaction progress variable are plotted for the y-z planes orthogonal to the direction of the mean flow as shown in Figure 7. On the plains closer to the reactants (7(a)) and products (7(d)) regions, both PDFs show the same distribution. However, inside the flame brush, the β-PDF predicts higher values of local maximum as c^* approaches 1 (7(b) and 7(c)), which is most likely due to the higher burning rates predicted by the β-PDF.

Figure 8 shows the predicted contours of species mass fraction for the turbulent premixed flame in the x-z plane and at $y = 0$. Comparison of Figures 8(a) and 8(b) for the predicted CO_2 mass fraction clarifies that choice of the β-PDF or modified laminar flame-based PDF does not have a strong influence on the mass fraction of major species, such as CO_2. This was also seen in the comparison of tabulated data for one dimensional laminar methane-air flames (3(a) and 3(b)). However, the H_2 and H mass fraction in Figures 8(c), 8(d), 8(e) and 8(f) clearly illustrate the stronger influence of PDF type on the prediction of minor species which agrees with Domingo et al.[8] and was also seen in the tabulated data (3(c) and 4(b)).

C. Laboratory Bunsen-Type Turbulent Premixed Flame

Large eddy simulation of a Bunsen-type burner is considered next. The burner has been studied experimentally by Yuen and Gülder.[38] The configuration consists of an inner nozzle diameter of 11.2 mm for generation of turbulent premixed flames stabilized by annular pilot flames. Rayleigh scattering was used to capture flame front images and calculate the temperature field. To measure the instantaneous velocity field, particle image velocimetry was used. The Bunsen flame considered in this work has the same turbulence scales and flame properties as the propagating premixed flame of the previous section, which are summarized in Table 1. For the simulations, a cylindrical domain is considered with diameter of 0.5 m and height of 0.1 m. The domain is discretized with a grid of 1,638,400 hexahedral cells. The pilot flame is approximated by a uniform flow of hot combustion products at a velocity of 16.81 m/s.

LES results for this flame have been obtained using both the β-PDF and modified laminar flame-based PDF with the PCM-FPI model. Three-dimensional views of the instantaneous flame surfaces are displayed in Figures 9(a) and 9(c) at $t = 4$ ms after the initiation of the simulation. This surface is plotted on the iso-surface of $\tilde{c} = 0.5$. Figures 9(b) and 9(d) show contours of instantaneous temperature for the same flame on a z-x plane. The initially planar flame near the inlet shows considerable development with downstream distance. It can be seen that the flame is well wrinkled and the shape of the flame is mostly convex towards the combustion products. Comparison of the LES results for the two PDFs shows that use of the β-PDF as opposed to the modified laminar flame-based PDF does not affect the overall shape of the flame significantly.

In order to compare the minor species mass fraction for two different PDFs, the mass fractions of OH and H are plotted along the z axis and in the middle of y and x axis (Figures 10(a) and 10(b)). For these minor species, the modified laminar flame-based PDF shows higher mass fractions compared to β-PDF.

To compare the results with the experimental data, the experimental flame is filtered using a top-hat filter with a width equal to two times the average cell size of the LES computations. 2D slices of the temperature field obtained from LES calculations are also averaged using 19 instantaneous snapshots of the numerical

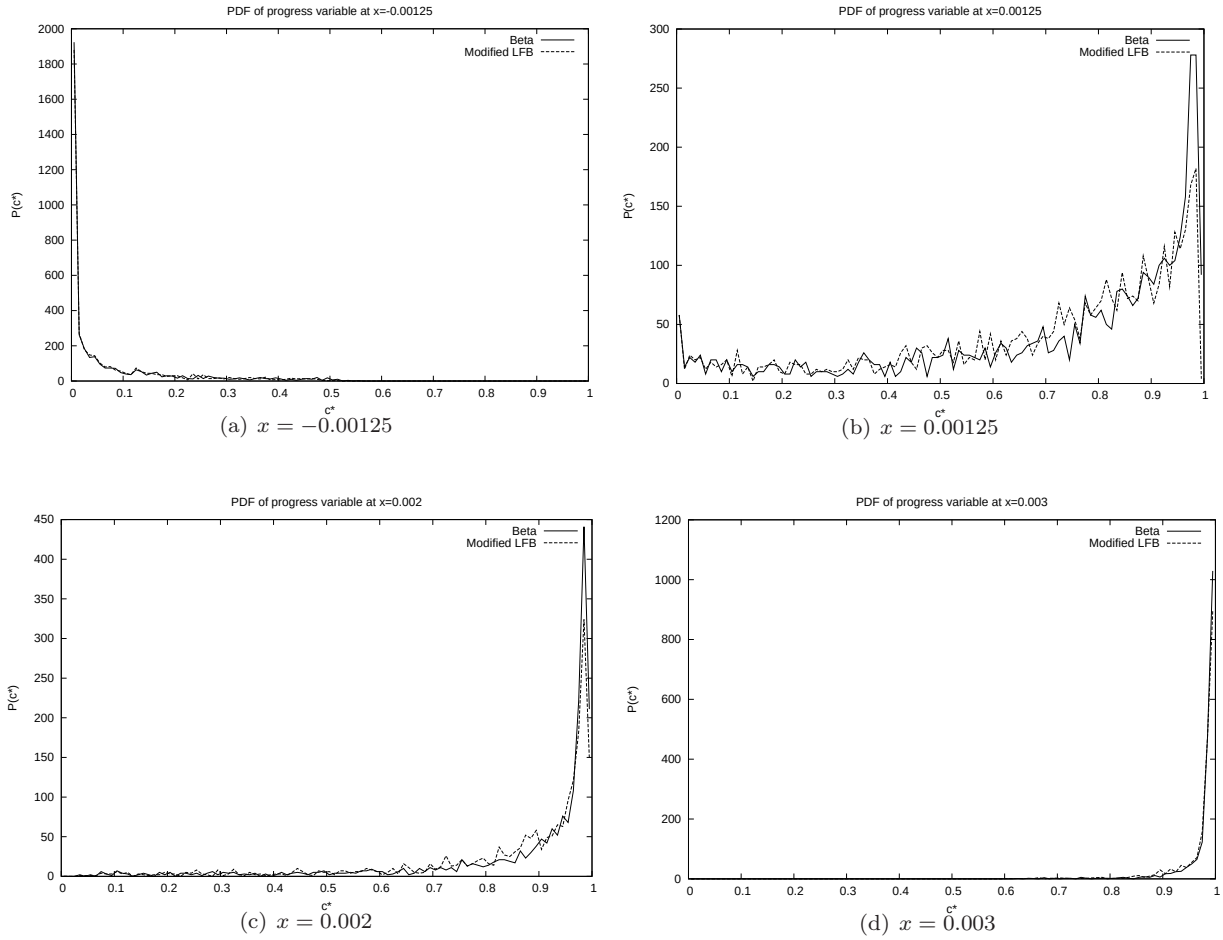

(a) $x = -0.00125$ (b) $x = 0.00125$

(c) $x = 0.002$ (d) $x = 0.003$

Figure 7. Distribution of reaction progress variable on y-z plains for cases with β-PDF and modified laminar flame-based PDF at $t = 1\,\mathrm{ms}$.

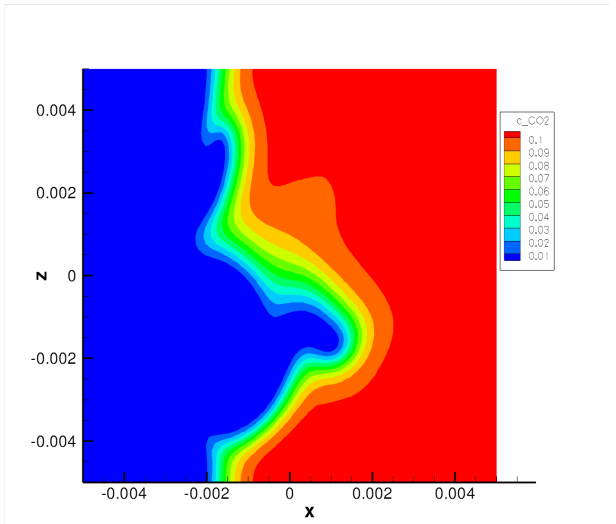

(a) β-PDF

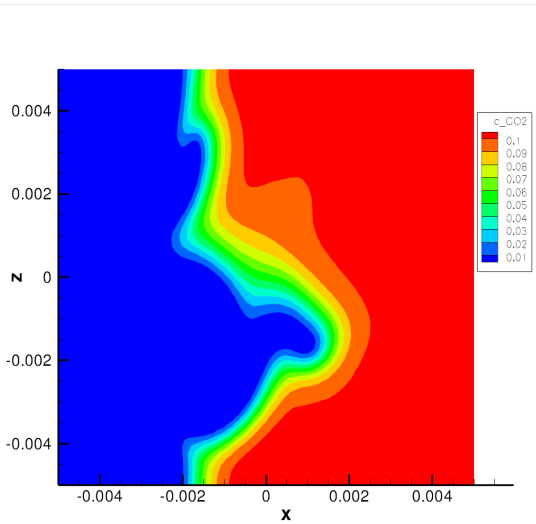

(b) Modified LFB PDF

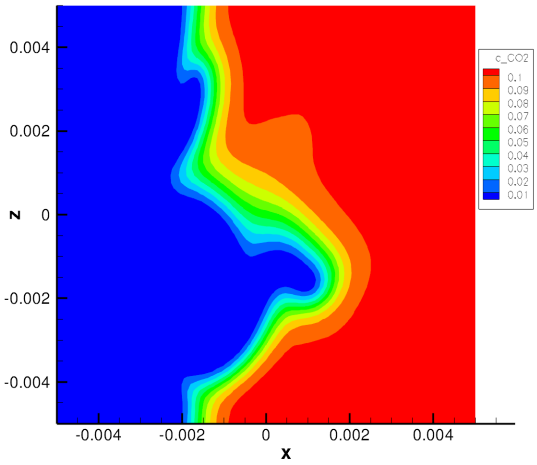

(c) β-PDF

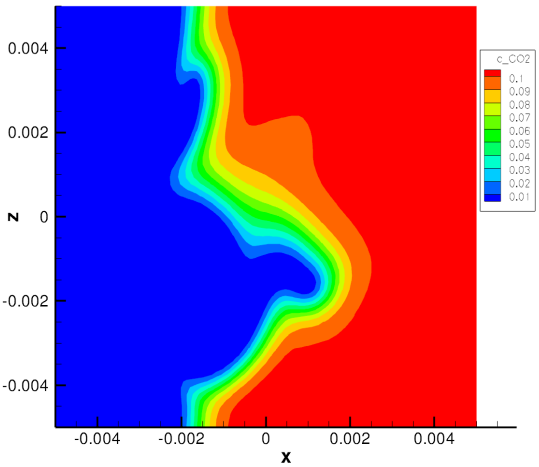

(d) Modified LFB PDF

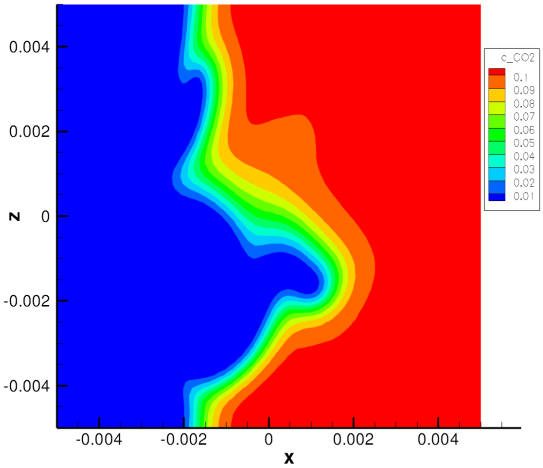

(e) β-PDF

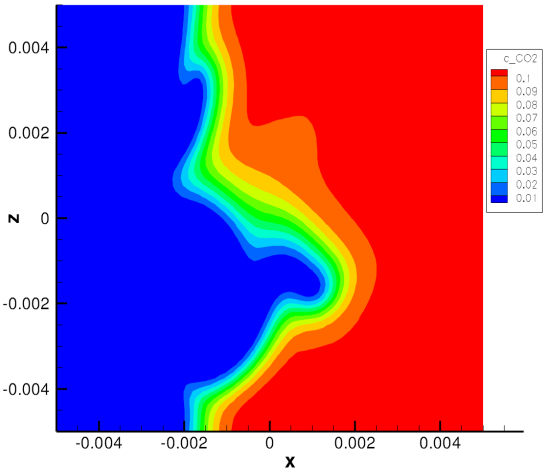

(f) Modified LFB PDF

Figure 8. Contours of species mass fraction in the x-z plain and at $y = 0$ for cases with β-PDF and modified laminar flame-based PDF at $t = 1$ ms.

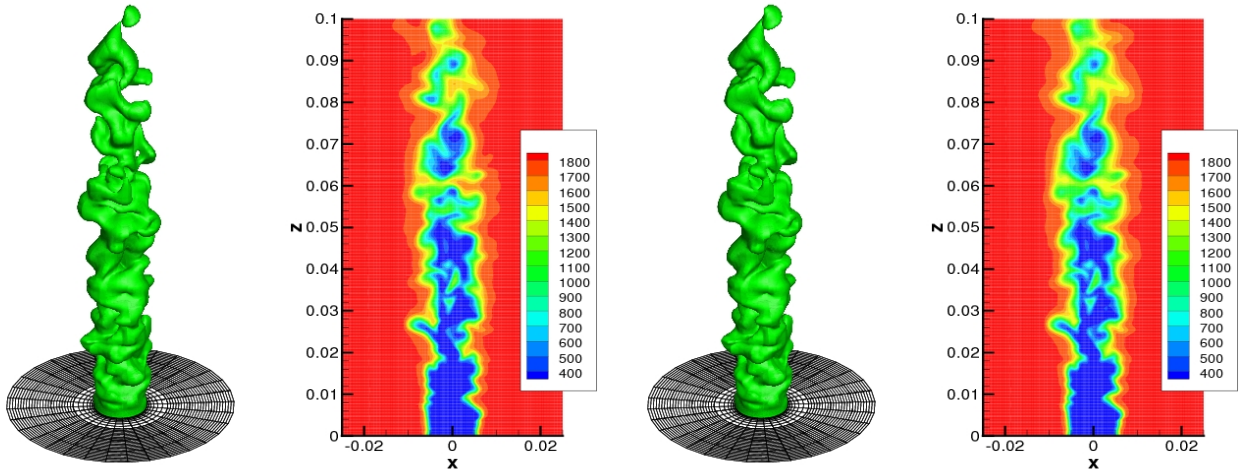

(a) β-PDF (b) β-PDF (c) Modified LFB PDF (d) Modified LFB PDF

Figure 9. Instantaneous flame isosurface $\tilde{c} = 0.5$ and contours of temperature on a plane at $t = 7\,\mathrm{ms}$ after the initiation of the simulation.

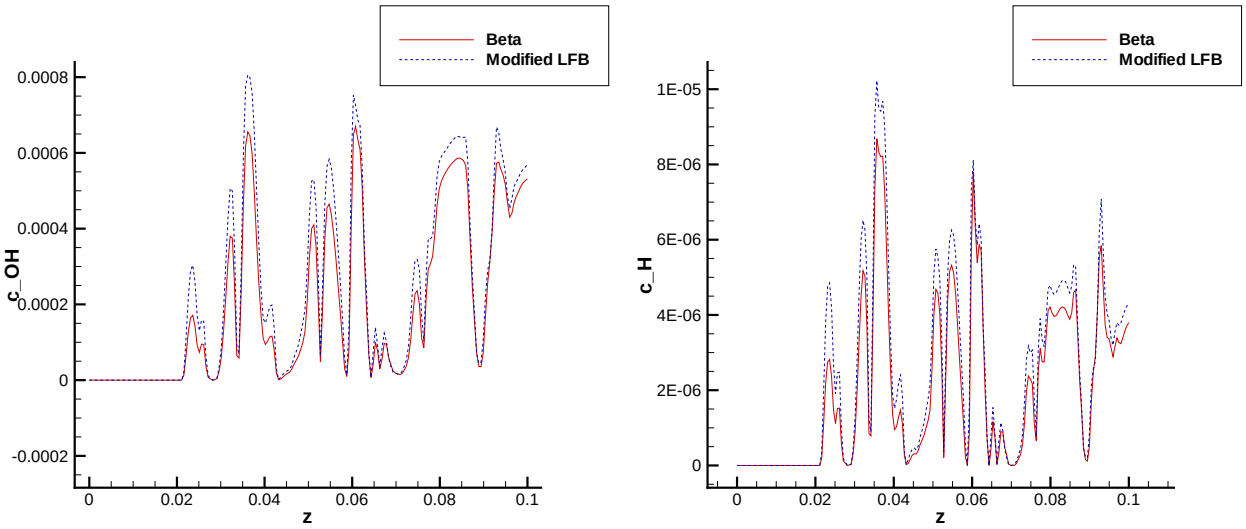

(a) (b)

Figure 10. Comparison of Y_{OH} and Y_{H} along the z axis and in the middle of x and y axis for two PDFs at $t = 7\,\mathrm{ms}$.

solution. The results for the instantaneous filtered temperature is shown in Figure 11(a). Figure 11(b) shows the contours of average $\langle c_T \rangle = 0.5$ from the simulations with PCM-FPI using β-PDF and modified laminar flame-based PDF and the map obtained from the Rayleigh scattering images of experimental data. The value c_T is defined as: $c_T = (T - T_u)/(T_b - T_u)$ where T is the local temperature and T_u and T_b are unburnt and burnt gas temperatures, respectively. It can be seen that there is a good agreement between the predicted results and the experiments in case of flame height and the overall shape of the flame. The modified laminar flame-based predicts slightly higher flame height compared to the β-PDF, but overall the two PDFs produce very similar predictions.

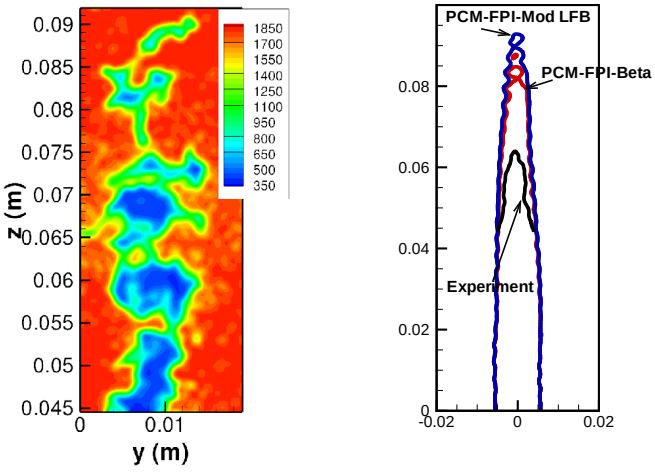

(a) (b)

Figure 11. Instantaneous filtered temperature from the experimental data and contours of $\langle c_T \rangle = 0.5$ from the experiments and simulations using PCM-FPI with β-PDF.

Comparison of the measured and predicted PDFs of flame front curvature corresponding to a progress variable $\langle c_T \rangle = 0.5$ is shown in Figure 12(a). It is apparent from the figure that PDFs calculated from experimental and predicted results are symmetric and Gaussian-like distributions. But both LES predictions show narrower PDFs as compared to the experimental results. LES filtering removes all the small scale structures which have higher curvature resulting a narrower PDF. By spatially filtering the experimental data, a better agreement can be obtained between experimental and LES results which supports the previous argument. Comparison between curvature PDFs for LES with β-PDF and modified laminar flame-based PDF does not show a distinct difference between LES calculations using these PDFs, which is consistent with the previous results (Figure 10) since the overall shape of the flames is not influenced significantly by the type of PDF.

The two-dimensional maps of flame surface density (FSD) is calculated using the method developed by Shepherd[39] for both LES and experimantal data. The 2D FSD values extracted from the simulations and the experiment are shown in Figure 12(b). There is very good agreement between the predicted calculations using LES with both PDFs and the experiments. It can be seen that the modified laminar flame-based PDF predicts a slightly lower FSD values than the β-PDF which is expected since the β-PDF is shown to overpredict the flame burning rate and consequently the flame surface density.

VIII. Concluding Remarks

LES of a freely propagating turbulent premixed flame and a Bunsen-type turbulent premixed flame has been carried out using the PCM-FPI approach. Three different presumed probability density functions for the reaction progress variable are tested. The tabulated data and the predicted LES solutions for the freely propagating flame configuration were compared using β-PDF and the modified laminar flame-based PDF. It is shown that the laminar flame-based PDF is not applicable in the present study where the flame is in the thin reaction zone regime. The tabulated data using the solution of one dimensional laminar flame shows higher reaction rate for β-PDF compared to the modified laminar flame-based PDF for high values of segregation factor. This is confirmed by comparison of turbulent burning rate in the predicted LES results

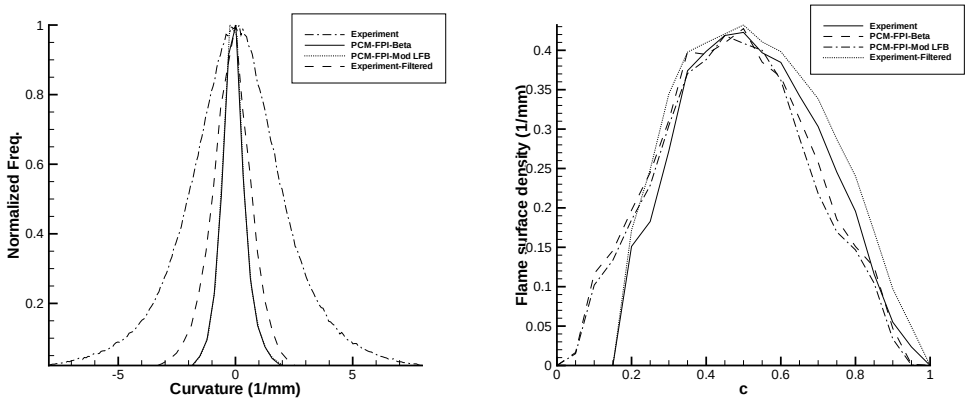

(a) (b)

Figure 12. 2D flame surface density and PDF of 2D curvature on a isosurface of $\langle c_T \rangle = 0.5$

where the burning rate for β-PDF is higher than the modified laminar flame based PDF. For the major species such as CO and CO_2, the two PDFs did not show any appreciable differences, both for the tabulated data and for the predicted LES solutions. However, for minor species such as H, H_2 and OH the difference is higher especially for high segregation factors. Direct numerical simulation of a propagating turbulent premixed flame presented above is performed for comparison between the predicted LES solutions with the β-PDF and the modified laminar flame-based PDF. For the Bunsen-type burner configuration, LES results were obtained using the PCM-FPI approach with β-PDF and modified laminar flame-based PDF. The results show good agreement with the experimental data. As was also observed for the propagating flame, the type of PDF used in the PCM-FPI approach does not seem to greatly influence the overall shape of the Bunsen burner flame. However, the minor species concentration were found to be more affected by PDF used in the tabulation procedure.

Acknowledgments

Computational resources for performing the calculations reported herein were provided by the SciNet High Performance Computing Consortium at the University of Toronto and Compute/Calcul Canada through funding from the Canada Foundation for Innovation (CFI) and the Province of Ontario, Canada.

References

[1]Pope, S. B., "PDF methods for turbulent reactive methods," *Prog. Energy Combust. Sci.*, Vol. 11, 1985, pp. 119–192.

[2]Gicquel, O., Darabiha, N., and Thévenin, D., "Laminar premixed hydrogen/air counterflow flame simulations using Flame Prolongation of ILDM with differential diffusion," *Proceedings of Combustion Institute*, Vol. 28, 2000, pp. 1901–1908.

[3]Fiorina, B., Gicquel, O., Vervisch, L., Carpentier, S., and Darabiha, N., "Premixed turbulent combustion modeling using tabulated detailed chemistry and PDF," *Proceedings of Combustion Institute*, Vol. 30, 2005, pp. 867–874.

[4]Galpin, J., Naudin, A., Vervisch, L., Angelberger, C., Colin, O., and Domingo, P., "Large-Eddy simulation of a fuel-lean premixed turbulent swirl-burner," *Combust. Flame*, Vol. 155, 2008, pp. 247–266.

[5]Domingo, P., Vervisch, L., and Veynante, D., "Large-Eddy simulation of a lifted methane jet flame in a vitiated coflow," *Combust. Flame*, Vol. 152, 2008, pp. 415–432.

[6]Subramanian, V., Domingo, P., and Vervisch, L., "Large eddy simulation of forced ignition of an annular bluff-body burner," *Combust. Flame*, Vol. 157, 2010, pp. 579–601.

[7]Bray, K. N. C., Champion, M., Libby, P. A., and Swaminathan, N., "Finite rate chemistry and presumed PDF models for premixed turbulent combustion," *Combust. Flame*, Vol. 146, 2006, pp. 665–673.

[8]Domingo, P., Vervisch, L., Payet, S., and Hauguel, R., "DNS of a premixed turbulent V flame and LES of a ducted flame using a FSD-PDF subgrid scale closure with FPI-tabulated chemistry," *Combust. Flame*, Vol. 143, 2005, pp. 566–586.

[9]Jin, B., Grout, R., and Bushe, W. K., "Conditional Source-Term Estimation as a Method for Chemical Closure in Premixed Turbulent Reacting Flow," *Flow Turbulence Combust.*, Vol. 81, 2008, pp. 563–582.

[10]Martin, M. P., Piomelli, U., and Candler, G. V., "Subgrid-scale models for compressible large eddy simulations," *Theoretical and Computational Fluid Dynamics*, Vol. 13, 2000, pp. 361–376.

[11]Knight, D., Zhou, G., Okong'o, N., and Shukla, V., "Compressible large eddy simulation using unstructured grids," Paper 98-0535, AIAA, January 1998.

[12]Fiotina, B., Baron, R., Gicquel, O., Thevenin, D., Carpentier, S., and Darabiha, N., "Modelling non-adiabatic partially

premixed flames using flame-prolongation of ILDM," *Combust. Theory Modelling*, Vol. 7, 2003, pp. 449–470.
[13]Michel, J. B., Colin, O., and Veynante, D., "Modeling ignition and chemical structure of partially premixed turbulent flames using tabulated chemistry," *Combust. Flame*, Vol. 152, 2008, pp. 80–99.
[14]Smith, G. P., Golden, D. M., Frenklach, M., Moriarty, N. W., Eiteneer, B., Goldenberg, M., Bowman, C. T., Hanson, R. K., Song, S., Gardiner, W. C., Lissianski, V. V., and Qin, Z., "GRI-Mech 3.0," http://www.me.berkeley.edu/gri_mech/.
[15]Fiorina, B., Gicquel, O., Vervisch, L., Carpentier, S., and Darabiha, N., "Approximating the chemical structure of partially premixed and diffusion counterflow flames using FPI flamelet tabulation," *Combust. Flame*, Vol. 140, 2005, pp. 147–160.
[16]Veynante, D. and Vervisch, L., "Turbulent Combustion Modeling," *Progress in Energy and Combustion Science*, Vol. 28, 2002, pp. 193–266.
[17]Goodwin, D. and Moffat, H. K., "Cantera," http://www.cantera.org.
[18]Ribert, G., Champion, M., Gicquel, O., Darabiha, N., and Veynante, D., "Modeling nonadiabatic turbulent premixed reactive flows including tabulated chemistry," *Combust. Flame*, Vol. 141, 2005, pp. 271–280.
[19]Salehi, M. M. and Bushe, W. K., "Presumed PDF mode;ing for RANS simulation of turbulent premixed flames," *Combust. Theory Modelling*, Vol. 14, 2010, pp. 381–403.
[20]Ivan, L. and Groth, C. P. T., "High-Order Central ENO Finite-Volume Scheme with Adaptive Mesh Refinement," Paper 2007-4324, AIAA, June 2007.
[21]Ivan, L. and Groth, C. P. T., "High-Order Central ENO Finite-Volume Scheme for the Advection-Diffusion Equation," *Proceedings of the 16th Annual Conference of the CFD Society of Canada, Saskatoon, Saskatchewan, Canada, June 9–11, 2008*, CFD Society of Canada, 2008.
[22]Gao, X. and Groth, C. P. T., "A Parallel Adaptive Mesh Refinement Algorithm for Predicting Turbulent Non-Premixed Combusting Flows," *Int. J. Comput. Fluid Dyn.*, Vol. 20, No. 5, 2006, pp. 349–357.
[23]Gao, X. and Groth, C. P. T., "Parallel Adaptive Mesh Refinement Scheme for Three-Dimensional Turbulent Non-Premixed Combustion," Paper 2008-1017, AIAA, January 2008.
[24]Northrup, S. A. and Groth, C. P. T., "Solution of Laminar Diffusion Flames Using a Parallel Adaptive Mesh Refinement Algorithm," Paper 2005–0547, AIAA, January 2005.
[25]Barth, T. J., "Recent Developments in High Order K-Exact Reconstruction on Unstructured Meshes," Paper 93-0668, AIAA, January 1993.
[26]Roe, P. L., "Approximate Riemann Solvers, Parameter Vectors, and Difference Schemes," *J. Comput. Phys.*, Vol. 43, 1981, pp. 357–372.
[27]Liou, M.-S., "A Sequel to AUSM, Part II: AUSM$^+$-up for all speeds," *J. Comput. Phys.*, Vol. 214, 2006, pp. 137–170.
[28]Coirier, W. J. and Powell, K. G., "An Accuracy Assessment of Cartesian-Mesh Approaches for the Euler Equations," *J. Comput. Phys.*, Vol. 117, 1995, pp. 121–131.
[29]Gordon, S. and McBride, B. J., "Computer Program for Calculation of Complex Chemical Equilibrium Compositions and Applications I. Analysis," Reference Publication 1311, NASA, 1994.
[30]McBride, B. J. and Gordon, S., "Computer Program for Calculation of Complex Chemical Equilibrium Compositions and Applications II. Users Manual and Program Description," Reference Publication 1311, NASA, 1996.
[31]Wilke, C. R., "A Viscosity Equation for Gas Mixtures," *J. Chem. Phys.*, Vol. 18, 1950, pp. 517–519.
[32]Gardiner, W. C., *Combustion Chemistry*, Springer-Verlag New York Inc., Boca Raton, 1984.
[33]Rogallo, R. S., "Numerical Experiments in Homogeneous Turbulence," NASA Technical Memorandum 81315, 1981.
[34]Pope, S. B., *Turbulent Flows*, Cambridge University Press, 2000.
[35]Peters, N., "The turbulent burning velocity for large-scale and small-scale turbulence," *J. Fluid Mech.*, Vol. 384, 1999, pp. 107–132.
[36]Aspden, A. and Nikiforakis, N., "Analysis of Implicit LES Methods," *Comm. App. Math. and Comp. Sct.*, Vol. 3, 2008, pp. 103–126.
[37]Vicquelin, R., Fiorina, B., Darabiha, N., Gicquel, O., and Veynante, D., "Coupling tabulated chemistry with Large Eddy Simulation of turbulent reactive flows," *C. R. Mecanique*, Vol. 337, 2009, pp. 329–339.
[38]Yuen, T. and Gülder, O., "Premixed turbulent flame front structure investigation by Rayleigh scattering in the thin reaction zone regime," *Proceedings of Combustion Institute*, Vol. 32, 2009, pp. 1747–1754.
[39]Shepherd, I., "Flame surface density and burning rate in premixed turbulent flames," *In Proc. of Combust. Inst.*, Vol. 26, 1996, pp. 373–379.